PHYSICAL REVIEW MATERIALS **2**, 123604 (2018)

Electronic properties of low-Σ grain boundaries in InAs

Altynbek Murat,[1] Masahiko Matsubara,[1] Binh-Minh Nguyen,[2] and Enrico Bellotti[1,*]
[1]*Department of Electrical and Computer Engineering, Boston University, 8 St. Mary's Street, Boston, Massachusetts 02215, USA*
[2]*HRL Laboratories, 3011 Malibu Canyon Road, Malibu, California 90265, USA*

(Received 6 June 2018; revised manuscript received 30 November 2018; published 27 December 2018)

We employ first-principles density functional theory to investigate the electronic and structural properties of grain boundaries (GBs) in InAs. In particular, we study the energetics and passivation mechanisms of representative low-Σ GBs, including Σ3(111), Σ3(112), Σ5(120), and Σ5(130), to establish their relative stability and experimental feasibility. We find that the symmetric-tilt twin-boundary Σ3(111) GB is the most stable GB, in excellent agreement with our experimentally characterized GB structures in InAs. In addition to our theoretically predicted GB structures, we systematically study and analyze different configurations of complex multifold experimentally observed InAs GB structures. We discuss the effect of different passivations and doping mechanisms on the electronic properties of the GBs. Understanding the exact nature of the GB electronic structure and stability, as well as their passivation mechanisms is a key step for the further development of InAs based optoelectronic devices on silicon and other heterogeneous large-area substrates.

DOI: 10.1103/PhysRevMaterials.2.123604

I. INTRODUCTION

Indium arsenide based semiconductor alloys, such as InGaAs and InAsSb, are widely employed in the design of laser diodes and infrared detectors due to their optical and electrical properties [1–6]. For high performance applications, lattice matched structures, grown on InP or GaSb substrates, are used due to the high material quality and low defect density that can be obtained. Even in the case of lattice mismatched substrates, the ability to grow elastically strained material leads to device-grade epitaxial layers. In the case of low-cost applications or heteroepitaxial growth on substrates that are significantly different from the material one wants to grow, the crystallinity of the epitaxial layer is significantly degraded. Interfacial defects, dislocations, and polycrystalline region can nucleate and deteriorate the material's optical and electrical properties. In the specific case of InAs, it is desirable, for a number of applications involving low-cost infrared detectors, to be able to grow device structures on large area silicon wafer where the read-out integrated circuit (ROIC) is fabricated. As a result of the large lattice mismatch between silicon and InAs, the overlayer exhibits a polycrystalline structure in which crystalline regions (grains) are separated by defective boundaries.

Grain boundaries (GBs) between adjacent crystalline regions are complex extended defects [7–12] and very challenging to eliminate. Furthermore, they impact not only the electronic properties of the material but also the device operation [8,13]. Consequently, if it is not feasible to eliminate such GBs, one needs to understand their structure and associated electronic properties to try to mitigate their impact on device performance. For example, growth parameters can be optimized to obtain a specific type of GB that is less problematic than others, or one can try to passivate the dangling bonds in the GB's cores to eliminate possible trapping states. GBs have been studied in detail for semiconductors used in photovoltaic applications, where polycrystalline materials are widely employed and GBs are known to be both detrimental and beneficial to their efficiency [14,15]. For example, GBs in polycrystalline solar cell materials, such as CdTe and Cu(In,Ga)Se_2, can improve the solar cell performance if they act as a hole barrier that can reduce carrier recombination but can be detrimental if they create deep defect levels, which can act as recombination centers [14–22]. Moreover, the presence of GBs can be exploited to segregate native defects to improve materials quality for other device applications [23–25]. Similarly, controlling the GB size in thermoelectric materials can improve their performance as a result of the increased phonon scattering at the GBs [26,27]. GBs are very challenging to study theoretically due to their complex atomic structure [9,28] and their fundamental properties have not been fully investigated [13], except for a few cases of technologically relevant materials. To the best of our knowledge, GBs properties of polycrystalline zinc-blende InAs have not been studied, either theoretically or experimentally. Recently, a series of studies on GBs in CdTe, which has a similar zinc-blende structure as InAs, have been reported in the literature [29–31].

For a given GB, Σ is the ratio of the coincident sites lattice unit cell to the standard unit cell and it can be used to describe the GB structures. Based on the coincidence site lattice (CSL) theory [32], GBs with lower Σ values are expected to have lower formation energies. However, recent studies have shown that the Σ values cannot be used to predict the energies of broader range of GBs and can only be applicable to specific symmetric-tilt grain boundaries [33]. It has been found that the symmetric-tilt low-Σ GBs are the most stable GBs in CdTe, specifically the Σ3(111) and Σ3(112) GBs, and their atomic structures have been confirmed experimentally using

---

[*] bellotti@bu.edu

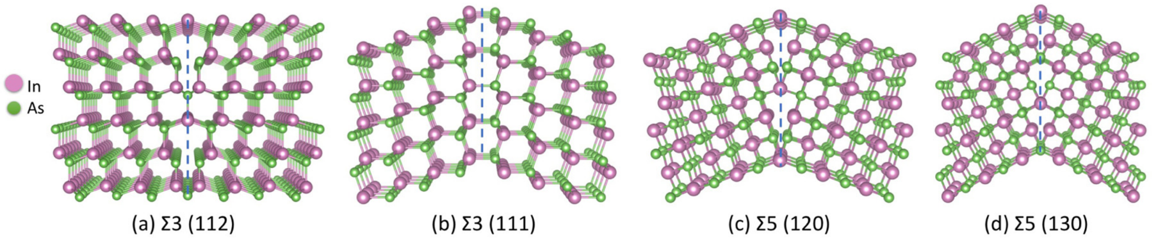

(a) Σ3 (112) (b) Σ3 (111) (c) Σ5 (120) (d) Σ5 (130)

FIG. 1. Atomic structures of representative low-Σ GBs in InAs: Σ3 (112), Σ3 (111), Σ5 (120), and Σ5 (130).

high resolution transmission electron microscopy (HRTEM) [28,30,34–38]. Furthermore, symmetric-tilt Σ3 GBs that were experimentally observed in CdTe have also been shown, by theoretical studies, to be the most stable GBs with lowest formation energies among the other GBs with higher Σ values [24,25].

In the case of InAs, no such study has been performed, consequently, it is not known whether Σ3(111) or Σ3(112) GBs are also the most stable GBs in zinc-blende InAs. Due to the technological importance of InAs for the design of infrared detectors, and the recent interest in large area deposition of InAs on silicon, it is important to undertake a systematic investigation of GBs in InAs, not only to identify their stable geometrical structures but also to establish their optoelectronic properties.

The aim of this work is twofold: (1) using first-principles density functional approach, we investigate the structural and electronic properties of low-Σ GBs in InAs; and (2) based on aberration-corrected scanning transmission electron microscopy (AC-STEM) analysis of InAs layers grown on silicon we identify the relevant GB structures and show that they match our theoretical predictions. In particular, we have investigated Σ3(111), Σ3(112), Σ5(120), and Σ5(130) GBs, shown in Fig. 1. These GB configurations were selected based on previous investigations on CdTe that shares the same zinc-blende crystal structure of InAs. We have studied the energetics and passivation mechanisms of these GBs to establish their relative stability and possible passivation approaches.

The manuscript is organized as follows. Section II describes the theoretical and experimental methods employed in this study. Section III will present the results and discuss them. Finally, Sec. IV will draw the conclusions of the work.

II. METHODS

This section describes the methodology employed to study the structural and electronic properties of the GBs and the experimental procedures used to grow and characterize the InAs layers.

A. Theoretical methods

The first-principles density functional electronic structure calculations have been performed using the projector augmented (PAW) [39] method implemented in the Vienna *ab initio* Simulation Package (VASP) [40]. For the formation energy calculations of the GBs, we use the generalized gradient approximation (GGA) in the Perdew, Burke, and Ernzerhof (PBE) parametrization for the exchange correlation functional [41]. A k-point grid of $4 \times 4 \times 1$ is used for the Brillouin zone sampling and a cutoff energy of 460 eV is used for basis function. All the structures were fully relaxed until the remaining force acting on each atom is less than 0.02 eV/Å. The optimized InAs lattice constant value is 6.001 Å, in good agreement with the experimental bulk value of 6.06 Å. We have tested several different corrections to the exchange/correlation energy functional in DFT including PBE+U and Heyd-Scuseria-Ernzerhof (HSE) hybrid functionals [42,43]. We find that PBE+U method with $U = 11.8$ eV correction with spin orbit coupling is the most appropriate and computationally efficient, providing an energy gap of 0.40 eV for bulk InAs. The $U = 11.8$ eV has been obtained by tuning the U value, such that it reflects the correct electronic structure of InAs that has been benchmarked based on the accurate HSE hybrid functional calculations. The symmetric-tilt GBs, as illustrated in Fig. 1, were modeled using a slab geometry within the supercell method, to avoid possible interaction between different GBs, as shown in Fig. 2. Surface dangling bonds in the supercells were passivated by pseudohydrogens with fractional charges of 3/4 e and 5/4 e for As and In, respectively [23]. Furthermore, the number of InAs layers and at least 20 Å vacuum on both sides of the GB were selected to minimize the effect of the supercell size on the GB electronic structure. The slab structures for the Σ3(111) GB contains 62 In and 62 As atoms with a slab size of 8.49 Å × 10.39 Å × 58.80 Å whereas the Σ3(112) GB contains 64 In and 64 As atoms with a size of 14.69 Å × 8.48 Å × 61.58 Å. Similarly, the Σ5(120) and the Σ5(130) slab structures have 50 In/As and 66 In/As atoms with slab sizes of 6.00 Å × 13.41 Å × 62.25 Å and 6.00 Å × 18.97 Å × 62.25 Å, respectively.

The formation energy (E_f) of the GBs has been calculated as $E_f = [E_{\mathrm{tot}}(\mathrm{GB}) - \sum_i n_i \mu_i]/\mathrm{S}$, where $E_{\mathrm{tot}}(\mathrm{GB})$ is the total energy of the slab system with the GB, n_i is the number of i atoms (i = In, As, pseudohydrogens), μ_i is the chemical potential of each i atom, and S is the GB area in the supercell.

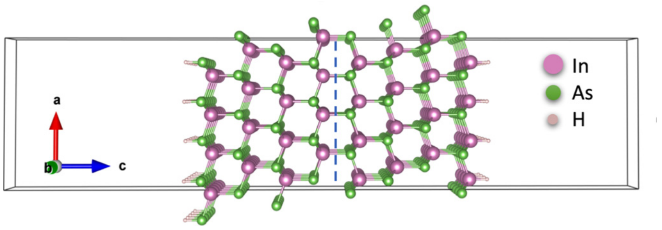

FIG. 2. Unit cell of Σ3(111) slab structure with single GB, periodic along the a and b directions and sufficient vacuum along the c direction.

The total energy of bulk InAs is equal to the sum of chemical potentials of In and As, $\mu_{\mathrm{In}} + \mu_{\mathrm{As}}$, when the system is in equilibrium. To avoid clustering of the elements, μ_{In} should be lower than that of bulk tetragonal In, and μ_{As} should be lower than that of bulk trigonal As. Chemical potentials of pseudohydrogen atoms are determined from the surface energies of the corresponding system [44]. However, for the calculation of relative formation energies, the explicit energy value of hydrogen is not needed because the comparison is relative and energies contributed from the fixed surface atoms cancel out. For the formation energy of the passivated systems, we employ the same approach as above but include the chemical potentials of the corresponding passivating atoms. For each passivating atom, we consider the corresponding elemental phases. For passivation with interstitial atoms, the atom is placed in between the wrong bonds in the core region and allowed to fully relax. For the case of combined vacancy and interstitial passivation, the vacancy is placed in between the wrong bonds as an interstitial atom. The resulting atomic positions of the representative Σ3(112) passivations are presented in the top panels of Fig. 5.

B. Experimental methods

InAs films were grown on Si (001) substrates by metal organic chemical vapor deposition (MOCVD) using trimethyl indium and arsine precursors. Prior to the growth, the Si substrates were cleaned with industrial standard RCA process. The InAs growth conditions were tuned for optimal structural properties (via x-ray diffraction, electron microscopy characterizations) while maintaining the low growth temperature constraints ($T \approx 425\,^{\circ}\mathrm{C}$) for compatibility with future integration with read out integrated circuits on silicon [45]. The InAs layers grown on Si (001) substrates are only relaxed at the cost of the grain boundaries, thus, we do not expect any significant effect on the standard bulk InAs structure in the experimental material. Specimens for transmission electron microscopy (TEM) were prepared by focus ion beam milling using gallium ions. Aberration-corrected scanning transmission electron microscopy (AC-STEM) was used to observe InAs crystal structures with atomic resolution under high-angle annular dark field (HAADF) and bright field modes.

III. RESULTS AND DISCUSSION

We start our analysis by investigating the atomic structures of a selected number of low-Σ GBs in InAs and systematically establish their stability. We have selected these structures based on the well known stable low-Σ GB configurations in CdTe material that are theoretically studied and experimentally observed [29–31,34]. Subsequently, based on images of GBs obtained by AC-STEM analysis of the InAs that have been grown and characterized, we identify both single and multiple GBs and match them to the theoretically predicted structures. Figure 1 presents the atomic structures of representative Σ3(112), Σ3(111), Σ5(120), and Σ5(130) symmetric-tilt GBs considered in this work. The Σ3(112), Σ5(120), and Σ5(130) InAs GB structures have a core (a hollow region with dangling bonds) at the boundary with cation–cation or anion–anion wrong bonds, whereas the Σ3(111) GB does not have any wrong or dangling bonds, as shown in Fig. 3(c). For example, Σ3(112) GBs can manifest either as As-core structure with As-As wrong bonds, as in Fig. 3(a), or In-core structure with In-In wrong bonds, shown in Fig. 3(b). We will use the As/In-core nomenclature to refer to these structures throughout the text. Due to their energetics, wrong bonds of different kinds have different impact on stability and the electronic structure of the GB.

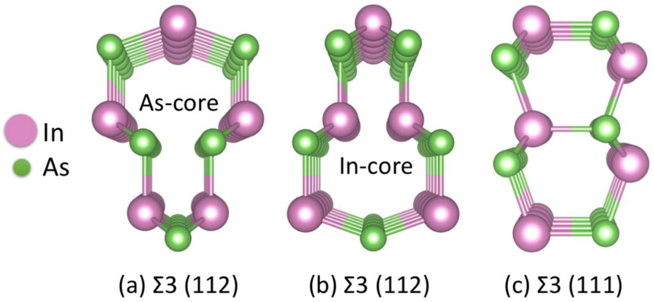

FIG. 3. Σ3(112) InAs GB structures with (a) As wrong bonds, As core and with (b) In wrong bonds, In core. (c) Σ3(111) InAs GB structure without any wrong bonds.

A. InAs Σ3(112) grain boundaries

To begin, we investigate the Σ3(112) GB in InAs as our starting model because it has been shown to be the dominant GB in the zinc-blende CdTe and similar II-VI semiconductors and it has been widely studied [30,34–38]. The structure of the Σ3(112) twin boundary in InAs is constructed by merging two (112) InAs planes together which results in a hollow region that is formed at the boundary. As mentioned before, the resulting structure can be either In-core [In atoms near the hollow region as in Fig. 3(b)] or As-core [As atoms near the hollow region Fig. 3(a)] stoichiometric structures with equal number of In and As atoms. Thus, their formation energies do not depend on the constituent chemical potentials. Based on the calculated electronic structure, both Σ3(112) GBs with different cores have metallic behavior with in-gap states induced by the wrong or dangling bonds. Furthermore, we find that the Σ3(112) GB with the As-core structure is more stable, with lower total energy than the In-core structure, with a difference of approximately 1.5 eV in total energy. This is due to the fact that the two As atoms in As-core have stronger bond compared to the two In atoms in the In-core. This is also reflected in the structural properties of the GB. The corresponding bond lengths for As–As and In–In wrong bonds are 2.56 and 2.87 Å, respectively. Consequently, in this work we will only focus on the lower-energy As-core Σ3(112) GB structure and investigate possible passivation strategies intended to mitigate the effects of the dangling bonds. Figure 4(a) presents the electronic structures of bulk InAs, and Figure 4(b) shows the calculated band structure of the As-core Σ3(112) InAs GB. Bulk InAs has a semiconducting behavior with calculated band gap of 0.40 eV. This is close to the experimental band gap of 0.41 eV, and the value calculated using HSE is of 0.40 eV with spin-orbit coupling and the amount of exact exchange was set to be 29%. The As-core Σ3(112) GB has a metallic behavior, as

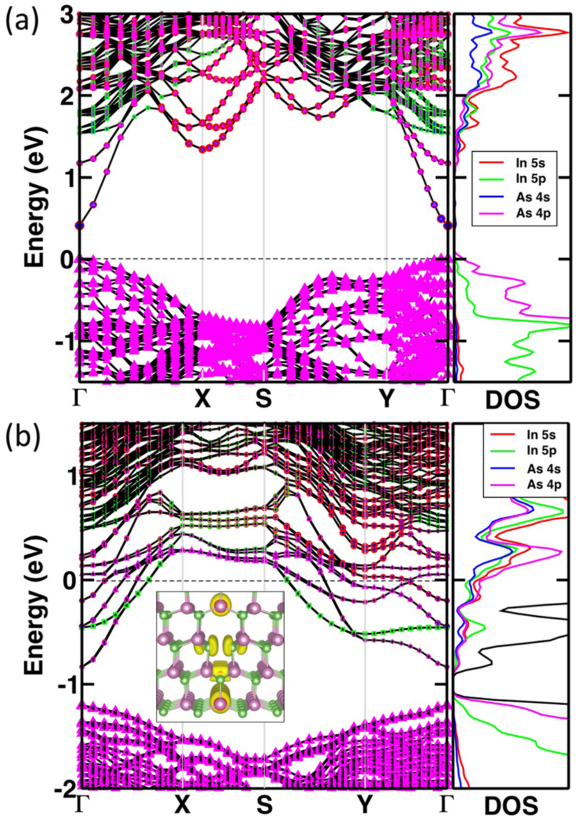

FIG. 4. Electronic band structure and partial density of states of bulk InAs (a) and Σ3(112) InAs As-core GB (b) with inset showing the partial charge density of the in-gap states. The Fermi level is set to 0 eV with dashed lines.

shown in Fig. 4(b), with no band gap with a Fermi level located in the conduction band. In addition to the As–As wrong bonds, this GB also presents three-coordinated In and five-coordinated As atoms at the hollow region. As a result, the partial density of states analysis reveals that the states in the gap are localized in the GB region and are indeed due to the wrong and dangling bonds. In order to mitigate the effect and saturate the dangling bonds responsible for the deep gap states, we investigate several passivation approaches and analyze their corresponding formation energies.

B. Passivation of InAs As-core Σ3(112) GBs

We have investigated several passivation approaches for the Σ3(112) As-core InAs GB structure, including self-passivation, doping with group-IV (C and Si) and group-II (Be and Zn) elements. The calculated electronic structure of the passivation approaches considered and their relative formation energies for the InAs Σ3(112) As-core GB are summarized in Figs. 5 and 6, respectively. We find that most of the approaches lead to imperfect passivation and the corresponding electronic structures are mostly metallic or have a very low energy gaps. Figures 5(a)–5(c) show the electronic structure and partial density of states along with their partial charge density results of self-passivations by In interstitial ($\mathrm{In_i}$), In vacancies (V_{In}), and a combination of V_{In} and $\mathrm{In_i}$, respectively. We find that self-passivations with both V_{In} [Fig. 5(a)] and $\mathrm{In_i}$]Fig. 5(b)] lead to imperfect passivation of As-As wrong bonds with In atom, resulting in a zero band gap. The partial charge density states, presented in the top panel by yellow bubbles, show extended in-gap states within the core region, as compared to the case without any passivation in the inset plot of Fig. 4(b). In contrast, the self-passivation by combined $\mathrm{In_i}$ and V_{In} results in a small band gap of 0.19 eV, as shown in Fig. 5(c), but deep levels still exist. The partial charge for the states in the gap are mostly from the As $4p$ states and are localized around the interstitial In-As bonds, whose length ranges from 2.68 to 2.73 Å.

Similarly, passivation by group-IV elements, such as $\mathrm{C_i}$ and $\mathrm{Si_i}$, leads once again to a metallic behavior without any band gap. Partial As passivation is seen in the case of Si, as shown in Fig. 5(e), and no As passivation for the case of for $\mathrm{C_i}$ as presented in Fig. 5(d). Only two As atoms are passivated by the silicon interstitial and the remaining two As atoms remain unpassivated. This can be seen from the charge density plot of the As–Si shown in Fig. 5(e). This results in As–Si bonds that have a length of 3.17 Å, while the ones of un-passivated As are 2.37 Å long. Finally, the states in the gap are mainly from As $4p$ and Si $3p$ states. In the case of $\mathrm{C_i}$, the in-gap states are mainly associated with C $2p$ states.

Passivation by group-II elements, for example $\mathrm{Be_i}$ and $\mathrm{Zn_i}$, leads to small band gaps with imperfect passivations. The calculated band gap values are 0.03 and 0.07 eV for $\mathrm{Be_i}$ and $\mathrm{Zn_i}$, respectively. For both cases, the partial charge states in the gap are from As $4p$ orbitals. The resulting As–Be and As–Zn bond lengths are 2.47 and 2.62 Å, respectively. Figure 6 presents a comparison of the formation energies of the passivations schemes used for the InAs Σ3 (112) GB with As-core structure. In Fig. 6, the formation energies for each passivant are plotted as a function of the In chemical potentials. Among all the passivants, $\mathrm{Zn_i}$ has the lowest formation energy but the resulting electronic structure has a zero band gap. The second lowest formation energy is the one of the system as-is, without any passivation. In contrast, self-passivation by combined $\mathrm{In_i}$ and V_{In} results in higher formation energy despite the small band gap of 0.19 eV [Fig. 5(c)], as a result this band-gap yielding approach is less stable. Similarly, the $\mathrm{Be_i}$ have higher formation energy than the as-is nonpassivated system and, as a result not-likely to be favorable. These results suggest that passivations based on other dopants may not be an effective approach to mitigate the impact of dangling bonds resulting from the GB core structure.

C. InAs Σ3(111) GBs

We have also investigated the InAs Σ3(111) GB structure that is shown in Fig. 7(c). The Σ3(111) GB is a symmetric-tilt twin-boundary structure that has been also observed experimentally in CdTe. The Σ3(111) GB structure has no wrong-bonds or dangling-bonds at the boundary. The lack of a hollow core with dangling bonds, makes the Σ3(111) GB a potential candidate for semiconducting behavior.

The atomic arrangement at the boundary resembles the one of a wurtzite crystal and, as a result, the GB can be considered a stacking fault between the wurtzite and zinc-blende InAs structures. The In-As bond length in the wurtzite-like region are only slightly different from the zinc-blende

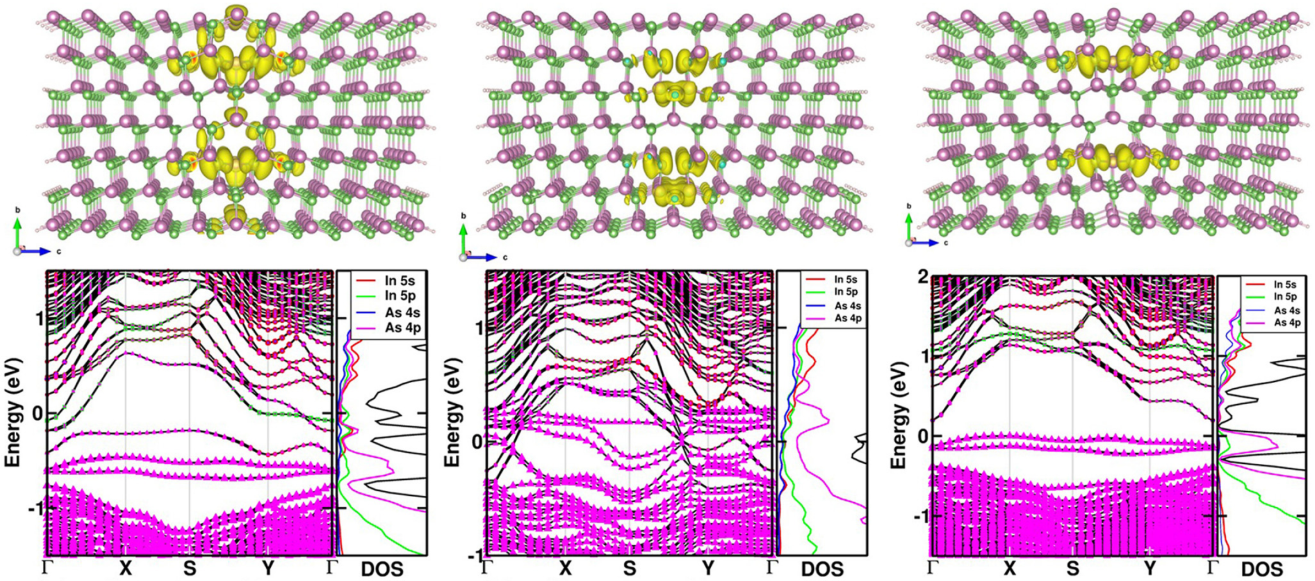

(a) Self-passivated by In_i (b) Self-passivated by V_{In} (c) Self-passivated by V_{in}-In_i

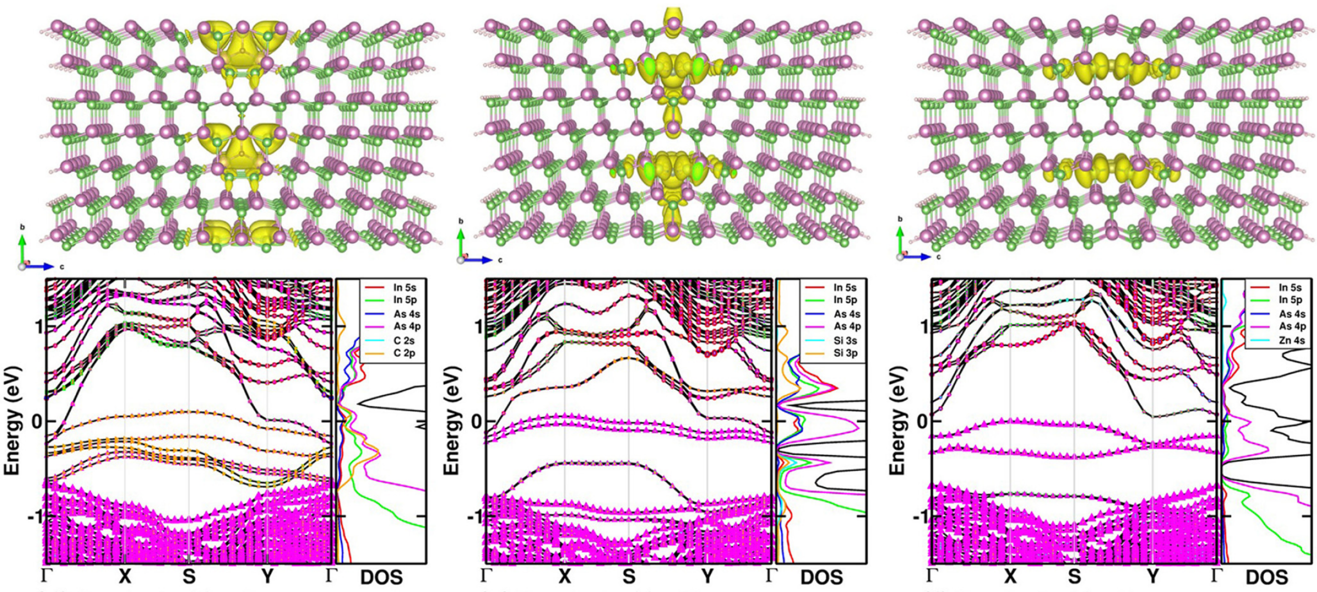

(d) Passivated by C_i (e) Passivated by Si_i (f) Passivated by Zn_i

FIG. 5. Representative passivation results for InAs Σ3 (112) GBs with As core structures, as calculated with PBE+U (=11.8) with spin orbit coupling (SOC). Magenta and green colors represent In and As atoms, respectively. Partial charge densities (yellow bubbles) for each case are plotted on top of the structures.

region. Consequently, the resulting formation energy, and resulting electronic structure of the GB, are expected to be not much different form the InAs bulk ones. From a direct comparison with the other kinds of GBs, we find that the Σ3(111) GB is the most stable one among all the studied GBs, with formation energy of 0.15 eV/Å^2. The formation energies for the Σ3(112), Σ5(120), and Σ5(130) GBs are 0.22, 0.36, and 0.23 eV/Å^2, respectively. We note that only the Σ3(111) GB shows a semiconducting behavior with an energy gap, whereas the Σ3(112), Σ5(120), and Σ5(130) GBs exhibit metallic behavior without an energy gap. Furthermore, we speculate that the electronic structure of the combined wurtzite and zinc-blende structure may cause an energy band offset, which can act as a diffusion barrier for the carriers in the material. The calculated electronic structure of the InAs Σ3(111) GB, shown in Fig. 7(d), results in a band gap of 0.68 eV, much larger than the one of bulk InAs. The Fermi level, which is set at 0 eV, lies within the energy gap and there are no induced deep gap states that could be detrimental to the electronic and optical properties. States closer to the Fermi energy originates mainly from the GB region, and the states that are detrimental to the electronic structure are far from the Fermi energy, as it can be seen in Fig. 7(d).

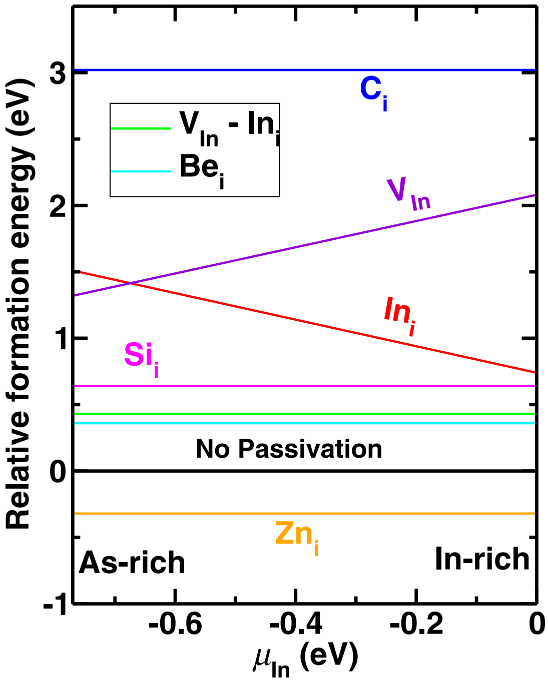

FIG. 6. Relative formation energies of InAs Σ3 (112) GBs with As-core structures.

From the characterization of InAs samples grown on silicon, we can directly obtain a number of possible GB configurations that are present between crystalline regions. Figure 7(a) presents a cross section of an exemplary InAs sample in which the crystalline regions and the GBs separating them can be immediately identified. From AC-STEM imaging obtained at the GB it is possible to evince the atomic structure and match it with the prototype GBs we have investigated. Figure 7(b) shows one of such AC-STEM pictures on which it is superimposed the atomistic GB model of a Σ3(111) GB. It is also interesting to notice that the large majority of GBs present in the sample, are of the Σ3(111) kind. In particular, in the single-crystal-like regrown films with improved crystallinity, almost all of the GBs were Σ3(111) type. This is consistent with the theoretical prediction that such GB has the lowest formation energy and as a result it is the most stable low-energy symmetric-tilt GB. It is also important to point out that Σ3(111) is also the most stable symmetric-tilt GB in other zinc-blende materials, for example, CdTe [28,30,34,37,38].

D. Complex Σ3(111) InAs GBs

Due to the complexity of polycrystalline materials and their grain arrangements, one should expect that multiple GBs be present in the same sample. These can be of the same kind, or an ensemble of different GB configurations. Consequently, it is important to evaluate the effect of multiple GBs and how their configurations affect the electronic structure of the material. Using the same kind of characterization approach, one can also obtain information on how multiple GBs are arranged and their atomic configuration. Since the Σ3(111) symmetric-tilt GB is the one with the lowest formation energy it is not surprising that multiple GB manifest in the material as combinations of multiple Σ3(111) GBs. Figure 8 presents three different configurations of GBs that have been experimentally observed during the characterization of the InAs sample material. These are multifold GBs in which the extent of region located between two GBs determines the atomic configuration at the GB. For each one of the three configurations in Fig. 8, we report the atomistic model in the upper panel and, in the lower panel, the AC-STEM picture. Figure 8(a) shows the structure of a double Σ3(111) InAs GB composed of two wurtzite regions positioned side by side. For simplicity, we classify this GB by indicating the two regions as type A and type B. Type B GB is basically the inverse structure of type A GB, where the type A GB is the same single Σ3(111) InAs GB which we discussed in Fig. 7(c). As a result, we refer to the structure in Fig. 8(a) as a AB type GB. Figure 8(b) presents the twofold Σ3(111) InAs GB, which consists of two Σ3(111) InAs GB interfaces, type A and type B, referred to as A-B GB. The two boundaries are not a periodic images of each other, but rather a combination of two inversely folded Σ3(111) InAs symmetric-tilt twin-boundaries, separated by 17 Å distance. We note that there is some strain in the experimental structure of this configuration,

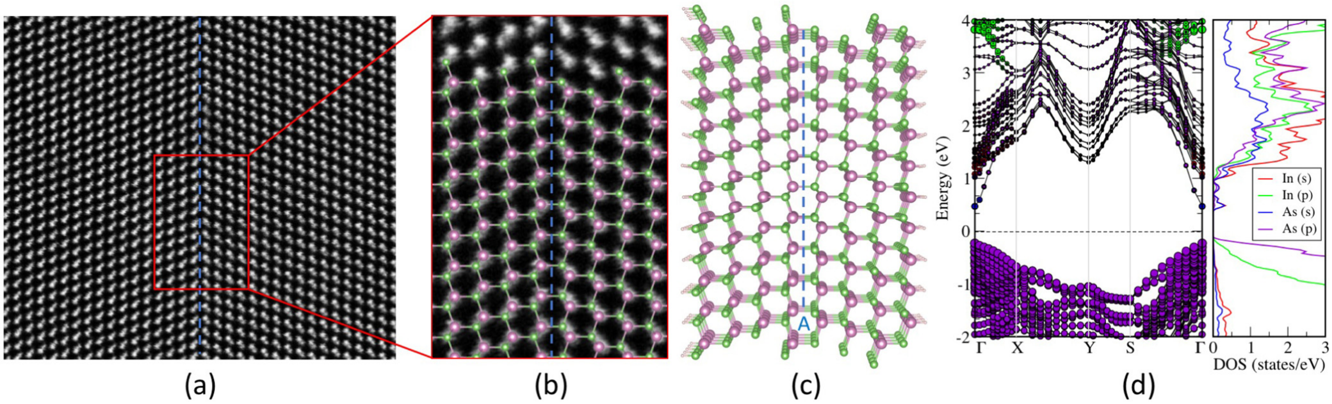

FIG. 7. (a) Experimental images of atomistic interfaces at the coalescence boundary of individually nucleated sites. (b) Theoretically predicted Σ3(111) InAs GB structure superimposed on the experimentally characterized 2 nm polycrystalline InAs GB structure (large/purple dots are In, small/green dots are As). (c) Atomic structure of Σ3(111) InAs GB and its corresponding (d) electronic band structure and partial density of states.

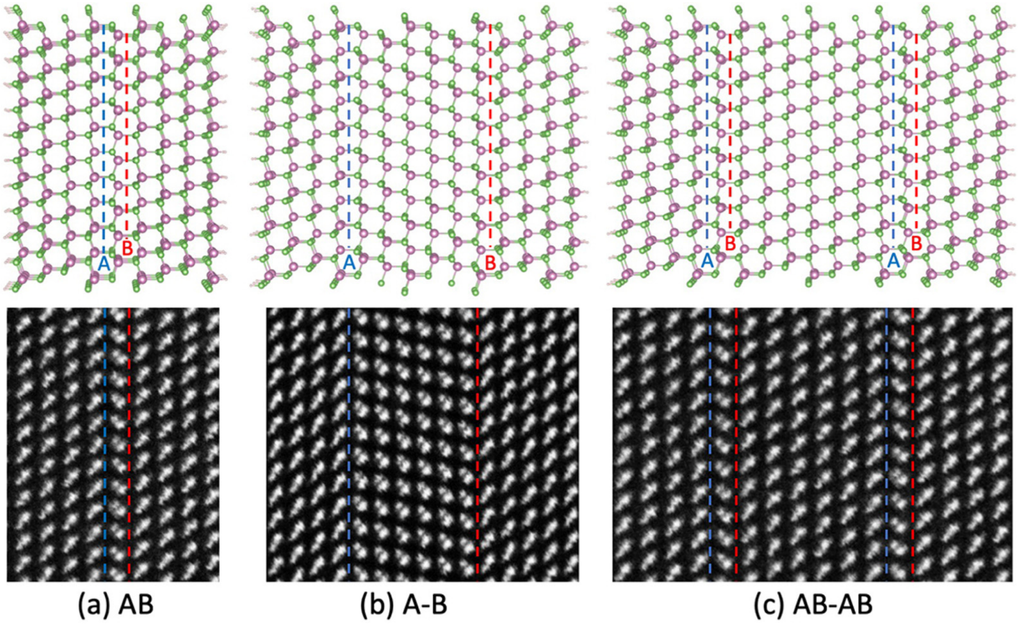

FIG. 8. (Top) Theoretical atomic structures of complex multi-fold Σ3(111) InAs GB with different configurations and boundaries. (Bottom) Matching experimentally characterized polycrystalline InAs GB structures (large/purple dots are In, small/green dots are As).

such that the middle region structure between the type A and type B boundaries is in slightly different angle than the opposite sides. Since the investigation of strain is beyond the scope of this work, we have not considered the strained structures in this work. Figure 8(c) presents the experimentally observed complex GB, which is composed by the repetition of two of the AB GBs, separated by 20 Å we will refer to this structure as the AB-AB GB. We should notice first that when the A-type and B-type GB are considered separately and isolated one from the other, they have the same electronic structures with the same band gap. However, when they are allowed to interact by changing the distance between them, they reveal a different electronic properties. Understanding how the electronic structure changes is critical in predicting the potential impact on material properties and eventually on device performance.

A possible way of comparing the three configurations in Fig. 8 is to look at the changes in the density of states at the GB region induced by the different configurations. Figure 9 presents the calculated density of states for the three experimentally observed GB configurations shown in Fig. 8. We find all three systems to be semiconducting with band gaps dependent on the GB and system size, as illustrated in Figure 9. The calculated band gap values are 0.65, 0.55, and 0.51 eV for the AB, A–B, and AB–AB GB structures, respectively. The calculated band gaps values indicate a trend for which the larger the system is the closer the band gaps get to the ideal bulk value. Furthermore, we find that the contribution to the states near the Fermi level is mainly from the GB states, whereas the states from the interface atoms are far from the Fermi level. Moreover, the partial density of states show that the valence band maximum (VMB) states are mainly from As(p)/In(p) states and the conduction band minimum (CBM) states are hybridized between the *s* and *p* states of both In and As.

E. Σ5(120) and Σ5(130) InAs GBs

While the Σ3(111) GB is the prevalent one in InAs, other GB configurations are also possible. We find that the Σ5(120) and Σ5(130) GBs have higher formation energies than the Σ3(111) and Σ3(112) structures, as a result they are not as stable as Σ3 GBs and we have chosen not to perform a detailed investigation. Similarly to the Σ3(112), the Σ5(120) and Σ5(130) GB structures have a hollow region at the interface between the crystalline regions with wrong and dangling bonds, as shown in Figs. 1(c) and 1(d). As expected, these bonds induce deep gap states, thus the electronic band structure for the both GB structures presents a metallic behavior without a band gap. For the case of Σ5(120), we find that the As-core structure has lower total energy than In-core by 1.1 eV. Furthermore, Σ5(130) GB is more stable than Σ5(120) GB by about 0.13 eV/A. Investigations of possible passivation mechanism for the Σ5 GBs are beyond the scope

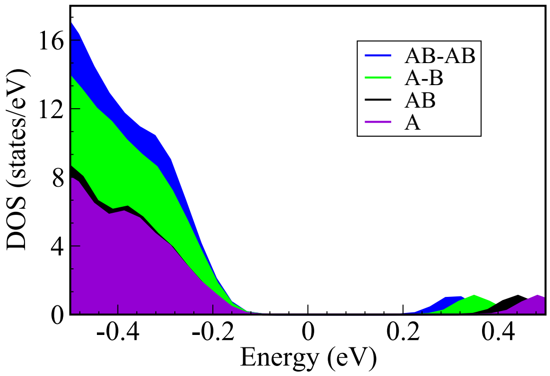

FIG. 9. Density of states for the representative four experimentally confirmed structures in Fig. 8.

of this work, mainly because the experimentally characterized GB atomic structures are primarily Σ3(111) GBs.

IV. CONCLUSIONS

We have employed a first-principles density functional methodology to systematically investigate the electronic and structural properties of stable GBs in InAs. In particular, we have studied the energetics and passivation mechanisms of low-Σ GBs, to evaluate their relative stability and to predict the structure of experimentally observed GBs in InAs. We have established that the symmetric-tilt Σ3(111) InAs GB is the most stable GB among all the studied GBs. From AC-STEM characterization of polycrystalline InAs samples we have found that the Σ3(111) GB is the most prevalent one compared to other low-Σ structures. This is in agreement with our theoretical prediction.

We find that the symmetric-tilt twin-boundary Σ3(111) GB is the most stable GB, in excellent agreement with our experimentally observed GB structures in polycrystalline InAs. We have also shown that the Σ3 GBs are more stable than the Σ5 GBs, as expected, since the former have been often found to be the most stable GB in zinc-blende materials.

Finally, we have studied the electronic band structures of the representative complex experimental GBs, such as multifold Σ3(111) GBs. We established a trend of multifold GB structures by systematically investigating different configurations of experimentally observed GBs in InAs. The results of these representative Σ3(111) GBs are expected to provide critical insight on the materials properties. We find that configurations of multiple Σ3(111) lead to a band gap that can be larger than the value normally observed in bulk InAs. A further understanding of the nature of the GB electronic structure as well as their passivation mechanism is a key step for the further development of large area devices made of polycrystalline InAs materials.

ACKNOWLEDGMENTS

This material is based upon work supported by the United States Air Force under Contract No. FA8650-16-C-7636. Any opinions, findings and conclusions or recommendations expressed in this material are those of the author(s) and do not necessarily reflect the views of the United States Air Force. This research was developed with funding from the Defense Advanced Research Projects Agency (DARPA). The views, opinions and/or findings expressed are those of the author and should not be interpreted as representing the official views or policies of the Department of Defense or the U.S. Government. The authors would like to thank Jay Lewis (DARPA-MTO), Whitney Mason (DARPA-MTO) for the support, Rajesh D. Rajavel (HRL), Christian Ratch, and Jonny Dadras (UCLA) for useful discussion.

[1] A. Haddadi, G. Chen, R. Chevallier, A. M. Hoang, and M. Razeghi, Appl. Phys. Lett. **105**, 121104 (2014).

[2] B. M. Nguyen, S. Bogdanov, S. A. Pour, and M. Razeghi, Appl. Phys. Lett. **95**, 183502 (2009).

[3] C. L. Tan and H. Mohseni, Nanophotonics **7**, 169 (2018).

[4] H. Wen and E. Bellotti, Appl. Phys. Lett. **107**, 222103 (2015).

[5] M. Desouky, A. M. Mahmoud, and M. A. Swillam, Sci. Rep. **7**, 15312 (2017).

[6] M. T. Soo, K. Zheng, Q. Gao, H. H. Tan, C. Jagadish, and J. Zou, Nano Res. **9**, 766 (2016).

[7] Y. Yan, W.-j. Yin, Y. Wu, T. Shi, N. R. Paudel, C. Li, J. Poplawsky, Z. Wang, J. Moseley, H. Guthrey *et al.*, J. Appl. Phys. **117**, 112807 (2015).

[8] P. Lejcek, Grain boundaries: Description, structure and thermodynamics, in *Grain Boundary Segregation in Metals*, Springer Series in Materials Science Vol. 136 (Springer, Berlin, Heidelberg, 2010).

[9] Z. Wang, M. Saito, K. P. McKenna, L. Gu, S. Tsukimoto, A. L. Shluger, and Y. Ikuhara, Nature (London) **479**, 380 (2011).

[10] A. Maiti, M. F. Chisholm, S. J. Pennycook, and S. T. Pantelides, Phys. Rev. Lett. **77**, 1306 (1996).

[11] M. Baram, D. Chatain, and W. D. Kaplan, Science **332**, 206 (2011).

[12] J. Kang, G. C. Glatzmaier, and S. H. Wei, Phys. Rev. Lett. **111**, 055502 (2013).

[13] L. Priester, *Grain Boundaries: From Theory to Engineering*, Springer Series in Materials Science Vol. 172 (Springer, Dordrecht, 2013).

[14] I. Visoly-Fisher, S. R. Cohen, K. Gartsman, A. Ruzin, and D. Cahen, Adv. Funct. Mater. **16**, 649 (2006).

[15] C. Persson and A. Zunger, Phys. Rev. Lett. **91**, 266401 (2003).

[16] W. K. Metzger and M. Gloeckler, J. Appl. Phys. **98**, 063701 (2005).

[17] J. Moseley, W. K. Metzger, H. R. Moutinho, N. Paudel, H. L. Guthrey, Y. Yan, R. K. Ahrenkiel, and M. M. Al-Jassim, J. Appl. Phys. **118**, 025702 (2015).

[18] W.-J. Yin, Y. Wu, S.-H. Wei, R. Noufi, M. M. Al-Jassim, and Y. Yan, Adv. Energy Mater. **4**, 1300712 (2014).

[19] I. Visoly-Fisher, S. R. Cohen, and D. Cahen, Appl. Phys. Lett. **82**, 556 (2003).

[20] C. Persson and A. Zunger, Appl. Phys. Lett. **87**, 211904 (2005).

[21] M. Gloeckler, J. R. Sites, and W. K. Metzger, J. Appl. Phys. **98**, 113704 (2005).

[22] M. Hafemeister, S. Siebentritt, J. Albert, M. C. Lux-Steiner, and S. Sadewasser, Phys. Rev. Lett. **104**, 196602 (2010).

[23] W.-J. Yin, Y. Wu, R. Noufi, M. Al-Jassim, and Y. Yan, Appl. Phys. Lett. **102**, 193905 (2013).

[24] C. Li, Y. Wu, J. Poplawsky, T. J. Pennycook, N. Paudel, W. Yin, S. J. Haigh, M. P. Oxley, A. R. Lupini, M. Al-Jassim *et al.*, Phys. Rev. Lett. **112**, 156103 (2014).

[25] V. Consonni, N. Baier, O. Robach, C. Cayron, F. Donatini, and G. Feuillet, Phys. Rev. B **89**, 035310 (2014).

[26] B. Poudel, Q. Hao, Y. Ma, Y. Lan, A. Minnich, B. Yu, X. Yan, D. Wang, A. Muto, D. Vashaee *et al.*, Science **320**, 634 (2008).

[27] K. Biswas, J. He, I. D. Blum, C.-I. Wu, T. P. Hogan, D. N. Seidman, V. P. Dravid, and M. G. Kanatzidis, Nature (London) **489**, 414 (2012).

[28] J. D. Major, Semicond. Sci. Technol. **31**, 093001 (2016).

[29] J.-H. Yang, W.-J. Yin, J.-S. Park, J. Ma, and S.-H. Wei, Semicond. Sci. Technol. **31**, 083002 (2016).

[30] C.-Y. Liu, Y.-Y. Zhang, Y.-S. Hou, S.-Y. Chen, H.-J. Xiang, and X.-G. Gong, Phys. Rev. B **93**, 205426 (2016).

[31] C. Sun, N. Lu, J. Wang, J. Lee, X. Peng, R. F. Klie, and M. J. Kim, Appl. Phys. Lett. **103**, 252104 (2013).

[32] S. Ranganathan, Acta Cryst. **21**, 197 (1966).

[33] D. L. Olmsted, E. A. Holm, and S. M. Foiles, Acta Mater. **57**, 3704 (2009).

[34] J.-S. Park, J. Kang, J.-H. Yang, W. Metzger, and S.-H. Wei, New J. Phys. **17**, 013027 (2015).

[35] Y. Yan, M. M. Al-Jassim, K. M. Jones, S. H. Wei, and S. B. Zhang, Appl. Phys. Lett. **77**, 1461 (2000).

[36] Y. Yan, M. M. Al-Jassim, and K. M. Jones, J. Appl. Phys. **94**, 2976 (2003).

[37] C. Sun, N. Lu, G. Lian, J. Wang, X. Peng, R. F. Klie, and M. J. Kim, Microsc. Microanal. **20**, 516 (2014).

[38] J. M. Oliveira, A. Malachias, C. A. Ospina, and S. O. Ferreira, J. Phys. Chem. C **118**, 1968 (2014).

[39] P. E. Blöchl, Phys. Rev. B **50**, 17953 (1994).

[40] G. Kresse and J. Furthmüller, Phys. Rev. B **54**, 11169 (1996).

[41] J. P. Perdew, K. Burke, and M. Ernzerhof, Phys. Rev. Lett. **77**, 3865 (1996).

[42] J. Heyd, G. E. Scuseria, and M. Ernzerhof, J. Chem. Phys. **118**, 8207 (2003).

[43] J. Heyd, G. E. Scuseria, and M. Ernzerhof, J. Chem. Phys. **124**, 219906 (2006).

[44] S. B. Zhang and S.-H. Wei, Phys. Rev. Lett. **92**, 086102 (2004).

[45] B. M. Nguyen, Y. Cao, A. J. Williams, D. E. Carrasco, J. R. Jenkins, L. Ray, T. J. De Lyon, S. Bui, B. Z. Nosho, and R. D. Rajavel, Proc. SPIE **10624**, 106240Z (2018).